Radicals from the Gas-Phase Pyrolysis of Catechol. 2. Comparison of the Pyrolysis of Catechol and Hydroquinone

ARTICLE *in* THE JOURNAL OF PHYSICAL CHEMISTRY A · SEPTEMBER 2010

Impact Factor: 2.69 · DOI: 10.1021/jp1054588 · Source: PubMed

5 AUTHORS, INCLUDING:

Lavrent Khachatryan
Louisiana State University
56 PUBLICATIONS **619** CITATIONS
SEE PROFILE

Rubik Asatryan
University at Buffalo, The State University …
52 PUBLICATIONS **367** CITATIONS
SEE PROFILE

Cheri Mcferrin
Louisiana State University
4 PUBLICATIONS **64** CITATIONS
SEE PROFILE

Barry Dellinger
Louisiana State University
145 PUBLICATIONS **2,275** CITATIONS
SEE PROFILE

Radicals from the Gas-Phase Pyrolysis of Catechol. 2. Comparison of the Pyrolysis of Catechol and Hydroquinone

Lavrent Khachatryan,*,† Rubik Asatryan,‡ Cheri McFerrin,† Julien Adounkpe,§ and Barry Dellinger†

Department of Chemistry, Louisiana State University, Baton Rouge, Louisiana 70803, Department of Chemistry and Environmental Science, New Jersey Institute of Technology, Newark, New Jersey 07102, and Université de Abomey Calavi, Faculté des Sciences Agronomiques, Bénin

Received: June 14, 2010; Revised Manuscript Received: July 30, 2010

Formation of radicals from the pyrolysis of catechol (CT) and hydroquinone (HQ) over a temperature range of 350−900 °C was studied using low-temperature matrix isolation electron paramagnetic resonance (LTMI EPR) spectroscopy. Comparative analysis of the pyrolysis mechanisms of these isomeric compounds was performed, and the role of semiquinone-type carrier radicals was studied. Pathways of unimolecular decomposition of intermediate radicals and molecular products were identified from the examination of the potential energy surface of catechol calculated at B3LYP hybrid density functional theory and composite CBS-QB3 levels. The results were compared with the experimental observations and mechanistic pathways previously developed for the pyrolysis of hydroquinone.

1. Introduction

Environmentally persistent free radicals (EPFRs) have been shown to be associated with combustion-generated particulate matter (PM) and airborne fine particles.[1] EPFRs are believed to have semiquinone-type structures, which are stable and relatively nonreactive in the atmosphere and capable of producing biologically damaging, reactive oxygenated species (ROS).[2] Hydroquinone (HQ) and catechol (CT) may be progenitors of semiquinone radicals, which have been implicated in the toxicity of cigarette smoke[3–7] and PM generated from the combustion of wood, coal, and other biomass.[8,9] However, the thermal degradation of CT and HQ has received modest attention in the literature,[10–14] and the toxicity of the resulting radicals is not fully understood.[7,15,16]

The formation of polycyclic aromatic hydrocarbons (PAHs) from the pyrolysis of CT under homogeneous, gas-phase conditions has been well studied,[11,17–19] and the product distribution from oxidative thermal degradation of CT under homogeneous[20,21] and catalytic conditions has been reported.[14] *Para*-benzoquinone (*p*-BQ) has been reported as the major decomposition product of the pyrolysis and oxidation of HQ.[20] The formation of *p*-BQ via *para*-semiquinone intermediate radical (*p*-SQ radical) was an a priori expected reaction pathway for HQ, and *p*-SQ radical was proven to be present in the pyrolysis of HQ at temperatures below 750 °C.[22,23] By analogy, *ortho*-semiquinone radical (*o*-SQ radical) was expected to be a radical intermediate in the *pyrolysis* of CT;[24] however, the corresponding molecular product, *ortho*-benzoquinone (*o*-BQ), was not observed in the experimental studies, which called into question whether *o*-SQ radical was formed.[12] However, *o*-BQ was observed in the gas-phase *oxidation*[20] and the surface-catalyzed thermal decomposition of CT.[14]

Recently, we reported formation of gas-phase radicals in the pyrolysis of both HQ[22,23] and CT[24,25] using the technique of low-temperature matrix isolation electron paramagnetic resonance (LTMI EPR) spectroscopy.[24] A split singlet EPR signal with a high *g*-value of 2.0052 was observed that is consistent with the EPR spectrum of radical pairs of *o*-SQ radical.[25] The hyperfine coupling in the EPR spectrum was assigned to the secondary effect of hydrogen bonding in the radical pairs formed while accumulating radicals at 77 K.

To gain insight into the mechanism of CT pyrolysis, different unimolecular decomposition pathways on the potential energy surface (PES) of CT were studied using CBS-QB3 multilevel and DFT individual level methods.[25,26] The lowest energy pathways involved conversion of CT to *ipso*- and α-CT isomers. Activation barriers for migration of corresponding hydroxyl hydrogen atoms to form *ipso*-CT and α-CT were calculated as 68.7 and 70.4 kcal mol^{-1}, respectively. O−H bond dissociation enthalpies of both isomers forming the same *o*-SQ radical were substantially lower than those in the initial CT molecule (viz., 79.0 kcal mol^{-1}).[25] Therefore, isomerization of the initial CT molecule was suggested to be more feasible than direct dissociation. This suggests the direct formation of *o*-BQ from CT is difficult and may explain its lack of formation. At the same time, the experimentally observed EPR spectrum of intermediate radicals with a high *g*-value was interpreted to be consistent with the calculated EPR spectrum of *o*-SQ radical.[25]

Recently, Altarawneh et al. published modeling results concerning detailed analysis of CT decomposition processes.[27,28] We are in general agreement concerning the principal channels for the pyrolysis initiation reactions, namely, the unimolecular isomerization channels of CT to α-CT and to *ipso*-CT, but the proposed initiation pathways differ. According to our previous calculations, the principal transition state, TS4, leading to the formation of *ipso*-CT (Scheme 1[25]) is as much as 20 kcal mol^{-1} lower in energy (68.7 kcal mol^{-1} at the CBS-QB3 composite level and 65.0 kcal mol^{-1} at the B3LYP level, at 298 K) than the TS localized for the same reaction by Altarawneh et al. using the same B3LYP method[28] (87.1 kcal mol^{-1} at 0 K, which is

* To whom correspondence should be addressed. E-mail: Lkhach1@lsu.edu.
† Louisiana State University.
‡ New Jersey Institute of Technology.
§ Université de Abomey Calavi.

10.1021/jp1054588
Published on Web 08/24/2010

SCHEME 1: Enthalpy Diagram for the Decomposition of Catechol (CT) at B3LYP/6-31G(d,p) (Bold Black) and CBS-QB3 (in Parentheses) Levels of Theory[a]

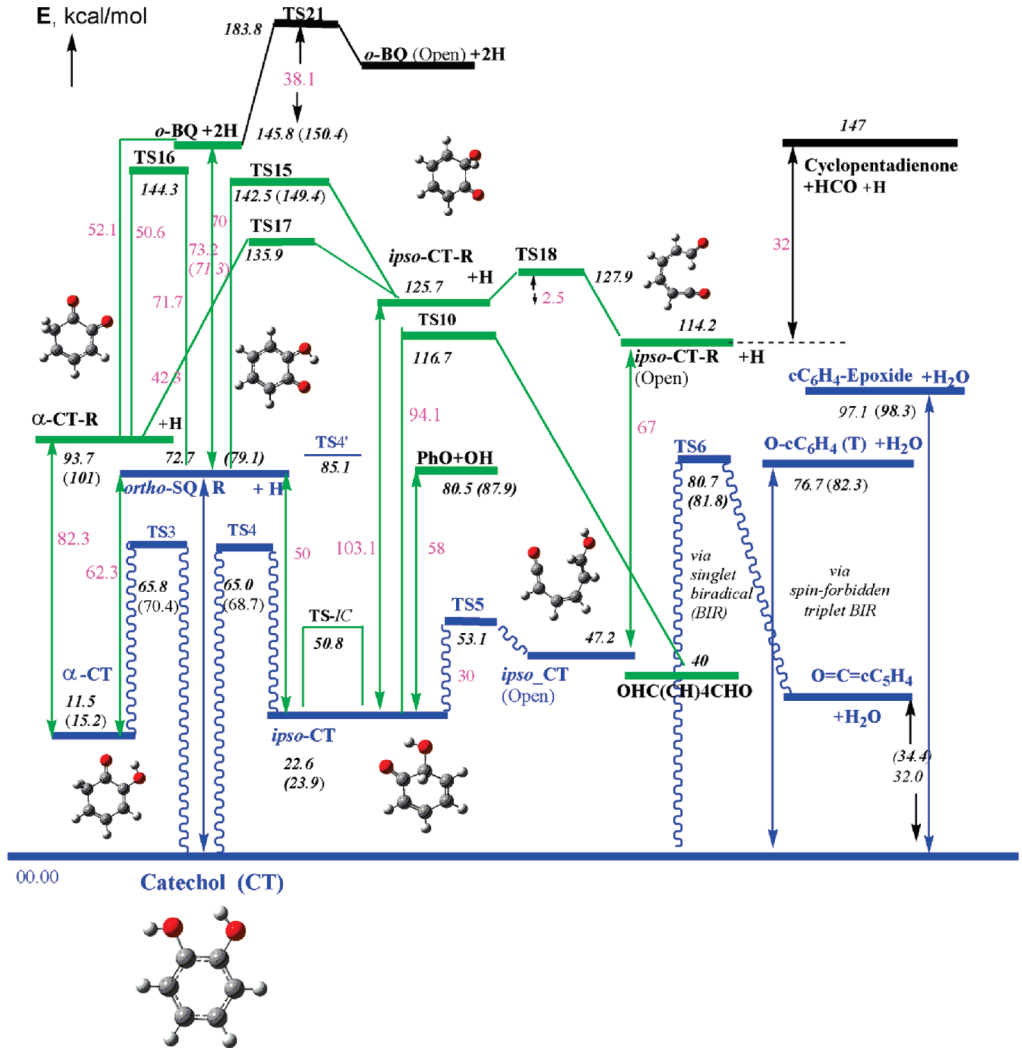

[a] Primary reactions are highlighted in blue, secondary reactions in green. Wavy lines in blue indicate direct formation and decomposition pathways with activation barriers. TS*i* are transition states associated with the corresponding reaction *i*. The abbreviation, R, refers to the radical.

ca. 2 kcal mol^{-1} higher than that of the 298 K value). Such a substantial difference in the energies of the initiation steps can result in remarkably different product formation rates.[28]

In this work, a detailed study of the formation of radicals from the pyrolysis of CT and HQ over a temperature range of 350−900 °C using LTMI EPR was performed. Quantum chemical calculations were processed to elucidate decomposition pathways of CT, formation and transformations of intermediate radicals, and formation of molecular products. The results were compared with the experimental observations and mechanistic pathways previously developed for the pyrolysis of HQ.

2. Procedures

Experimental Procedures. A detailed description of LTMI EPR can be found in some recent publications.[22,24] Briefly, the vapors of CT/HQ were introduced into a thermoelectrically heated, fused silica reactor (i.d. = 12 mm, length = 40 mm) at the desired temperature. Carbon dioxide gas was used as a carrier, and the residence time in the high temperature zone was 4 ms at a total pressure of 0.3 Torr. The gas flow (saturated by vapors of CT/HQ) exited the vaporizer, thermo-regulated at 50 °C, and entered the pyrolysis zone. Carbon dioxide is inert under these reaction conditions and does not affect radical formation. The delivery rate of CT/HQ was ∼10^{-3} mmol/min. The same carbon dioxide carrier gas was used as a supporting matrix to assist in the freezing of radicals. Pyrolysis products were condensed onto the coldfinger of the Dewar placed in the EPR cavity and cooled by liquid nitrogen. To avoid CT or HQ condensation on the walls, all transfer lines from the vaporizer to the coldfinger of the Dewar were maintained at 70 °C regardless of the pyrolysis reaction temperature.

EPR spectra were recorded on a Bruker EMX-20/2.7 EPR spectrometer (X-band) with dual cavities, modulation and microwave frequencies of 100 kHz and 9.516 GHz, respectively. The typical parameters were: sweep width 200 G, EPR microwave power of 0.1−20 mW, and modulation amplitude ≤4 G. Time constant and sweep time were varied. Values of *g*-factors were calculated using Bruker's WINEPR program, which is a comprehensive line of software, allowing control of the Bruker EPR spectrometer, data-acquisition, automation routines, tuning, and calibration programs on a Windows-based PC [http://us.bruker-biospin.com/brukerepr/winepr.html].

Experiments were also conducted to distinguish individual radicals in a complex mixture formed from the gas-phase pyrolysis of CT/HQ. These included annealing experiments, computer analysis of digitally stored spectra acquired over a

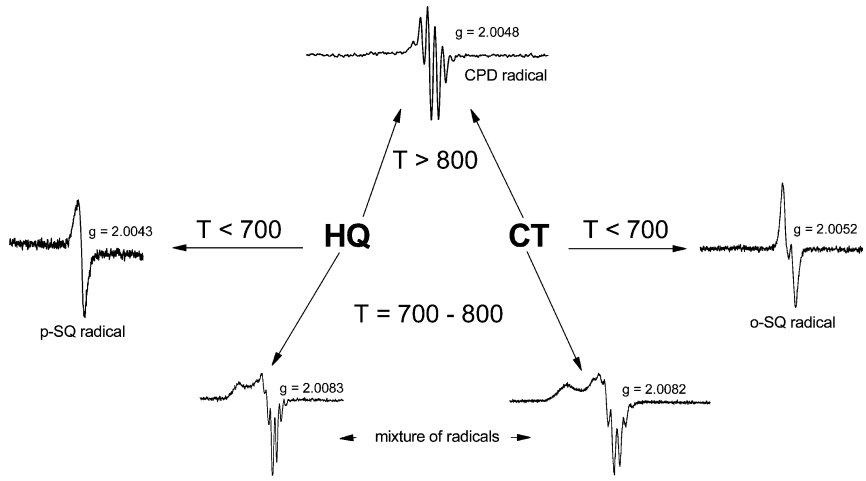

Figure 1. Comparison of radicals generated from pyrolysis of CT and HQ using LTMI EPR technique (EPR spectra of radicals were registered at liquid N_2 temperature).

wide temperature range of 350−900 °C. The annealing experiments (gradual warming of the Dewar by removing liquid nitrogen) resulted in the selective annihilation of the more reactive radicals such that the spectra of the more persistent, individual radicals in the mixture could be discerned.

Computational Procedures. Selected pathways on the PES of CT were initially calculated using hybrid B3LYP/6-31G(d,p) density functional theory[29,30] as implemented in the Gaussian 03 suite of programs.[31] Additional higher level calculations were performed to improve energetics of principal stationary points using CBS-QB3 composite level theory,[32] well recommended in the study of intricate PES.[33]

CBS-QB3 uses B3LYP functional for geometries and frequencies and combines the results of several electronic structure calculations and empirical terms to predict molecular energies to accuracies of ∼1 kcal mol^{-1}.[32] Geometries and frequencies were calculated at B3LYP/6-311G(2d,d,p) level. This basis set included 2d-functions on the second row elements, d-polarization function on the first row, and additional p-polarization function on hydrogen atoms. This p-polarization was included to result in better transition state structure for *hydrogen transfer reactions*.[32] Two additional calculations were used in the CBS-QB3 method to approximate higher order contributions: MP4(SDQ)/6-31+G(d(f),p) and CCSD(T)/6-31+G†). There were also *correction for spin contamination* (proportional to $\langle S^2 \rangle$) and size consistent higher order empirical correction. The CBS-QB3 method has an advantage of utilizing geometry and frequencies calculated at the *same level of theory*, namely, B3LYP/6-311G(2d,d,p), which is important for correct localization of TS structures.[32,33]

Transition states are characterized as having only one negative eigenvalue of Hessian (force constant) matrices. The absence of imaginary frequencies verifies that structures are true minima at their respective levels of theory. The intrinsic reaction coordinate (IRC) procedure is used for the identification of the connectivity of stationary points on the respective PES cross sections. The final scan points of IRC are additionally optimized to ensure that the reactions from the saddle points lead to the proper reactant and product. Spin contamination of the open-shell systems in this study was small as judged by the corresponding $\langle S^2 \rangle$ expectation values. In unrestricted B3LYP calculations, $\langle S^2 \rangle$ for radicals were less than 0.76 before and 0.75 after annihilation.

Abbreviated names are employed for molecules and radicals as described above. Black digits in Scheme 1 represent energies calculated at B3LYP/6-31G(d,p) level. Key structures on PES recalculated at CBS-QB3 level are presented in parentheses wherever applicable. TS*i* notations are used for transition states with "*i*" associated with the reaction numerations (vide infra). TS-IC is the transition state for interconversion reaction between two identical *ipso*-CT structures with an activation barrier of 28.2 kcal mol^{-1}.

3. Results and Discussion

Radicals from the Pyrolysis of CT and HQ. A summary of experimental results concerning the nature and the origin of radicals generated from the thermal pyrolysis of CT and HQ is presented in Figure 1. Two different types of radicals were identified from the gas-phase pyrolysis of CT/HQ over the temperature range of 350−900 °C. *p*-SQ radical, formed from HQ, and *o*-SQ radical, formed from CT pyrolysis, were dominant between 350 and 700 °C, whereas cyclopentadienyl (CPD) radicals dominated at high temperatures from 800 to 900 °C (Figure 1). At intermediate temperatures, 700−800 °C, mixtures of *p*-SQ + CPD, and *o*-SQ + CPD radicals were identified for HQ and CT, respectively. The identification

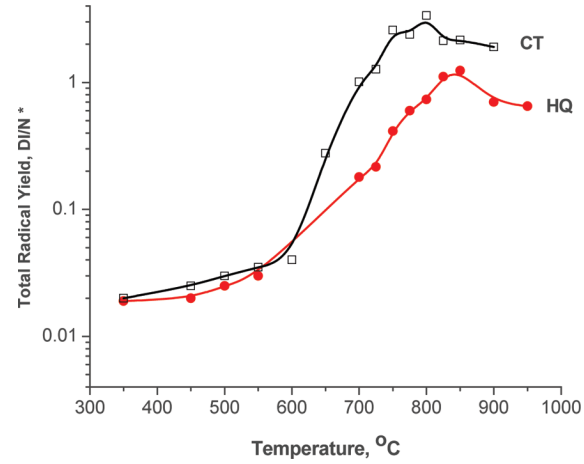

Figure 2. Comparison of temperature dependence of total radical yields from pyrolysis of CT and HQ at delivery rate ∼2.5 × 10^{-3} mmol/min in flowing CO_2 at 0.3 Torr pressure. * DI/N value is the double integrated (DI) intensity of the EPR spectrum that has been normalized (N) to account for the conversion time, receiver gain, number of data points and sweep width [http://www.bruker-biospin.com/winepr.html?&L = 0].

procedures were based on the annihilation and microwave power saturation experiments for the frozen radicals, and GC/MS analysis of pyrolysis products.[12,13,22,23,25]

Temperature Dependence of Total Radical Yields. Although the maximum concentration of radicals is achieved at lower temperature for CT (800 °C) than HQ (875 °C), the temperature dependences of the total radical yield are similar (Figure 2). CPD radical is the predominant active center above 800 °C for both compounds. The semiquinone radicals, *p*-SQ and *o*-SQ from HQ and CT, respectively, are dominant below 700 °C. As indicated in the introduction, *p*-BQ is the major molecular product from the pyrolysis of HQ,[13] but the analogous *o*-BQ was not observed from the pyrolysis of CT.[12] To address the somewhat unexpected result, different cross sections of the PES of the unimolecular decomposition pathways of CT were examined.

Primary Decomposition Channels (Initiation of Pyrolysis). ***Simple Bond Cleavage in CT.*** The simplest dissociation channel in CT includes O−H bond scission forming *o*-SQ radical, (Rxn 1). The bond dissociation enthalpy (BDE) calculated at 298 K at the B3LYP level (72.7 kcal mol^{-1}) is substantially lower than the dissociation limit calculated at the CBS-QB3 level (79.1 kcal mol^{-1}).

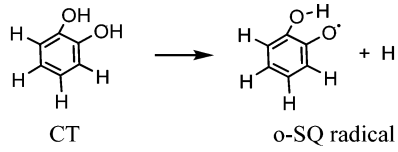

(1)

The BDE at the composite level, CBS-QB3, as well as values calculated by Altarawneh et al., based on isodesmic reactions,[27,28] are in good accord with the experimental BDE (81.6 ± 2.0 kcal mol^{-1}).[34]

According to the single level DFT calculations (Scheme 1), the first O−H dissociation reaction in CT (Rxn 1) is somewhat lower in energy (72.7 kcal mol^{-1}, B3LYP level) than the second O−H dissociation reaction, Rxn 2 (transformation of *o*-SQ radical to *o*-BQ with 73.2 kcal mol^{-1} BDE).

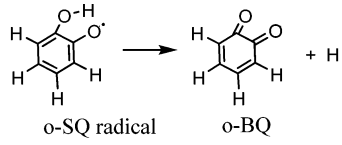

(2)

The difference between the BDEs for the two dissociation stages is reversed at the CBS-QB3 higher level of calculations (79.1 vs 71.3 kcal mol^{-1}) with a difference as high as 7.8 kcal mol^{-1}.

Isomerization of CT. The lowest energy products from the initial conversion (isomerization) of CT are identified as α-CT and *ipso*-CT isomers (TS3 and TS4 in Scheme 1).[25]

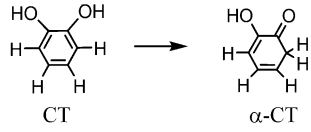

(3)

Both barriers to formation are substantially lower than the simple hydroxyl bond dissociation energy discussed above. The isomerization of CT to *ipso*-CT with a barrier of 65.0 kcal mol^{-1} and 68.7 kcal mol^{-1} at B3LYP and CBS-QB3 levels, respectively, is the lowest energy unimolecular pathway. Formation of α-CT, including migration of a hydrogen atom from an OH group to the neighboring carbon atom, has a slightly higher barrier (65.8 and 70.4 kcal mol^{-1}, at the B3LYP and CBS-QB3 levels, respectively). The difference between the two main isomerization channels is only 0.8 kcal mol^{-1} at the DFT level. However, it increases at higher CBS-QB3 composite level calculations. Note that CBS-QB3 involves energy calculations by CCSD(T) and higher order MP perturbation methods.[32] The barrier for the α-CT formation, calculated by Altarawneh et al., using the single level B3LYP method, was 67.1 kcal mol^{-1} at 0 K,[28] which is consistent with our value of 66.1 kcal mol^{-1} at 0 K using B3LY/6-31G(d,p) calculations (or 65.82 kcal mol^{-1} at 298 K as presented in Scheme 1). However, Altarawneh et al. calculated a very high activation energy for *ipso*-CT formation of 87.1 kcal mol^{-1} via transition state TSQ5.[28] Our values were only 65.4 kcal mol^{-1} at the B3LYP level and 69.1 kcal mol^{-1} at the CBS-QB3 level at 0 K.

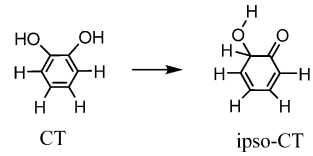

(4)

Due to the significance of the pathway for formation of *ipso*-CT, a detailed description of this channel is represented in Figure 3. It illustrates the transition state that we have localized and presented in the corresponding PE diagrams in our previous works.[25,26] This transition state (noted as TS4 in Scheme 1), which, in fact, is the lowest energy unimolecular channel for CT, is rather unique. Although the H^1 atom of the OH^1-group of CT transfers to the *ipso* carbon atom along the reaction coordinate, H^2 of the neighboring OH^2-group migrates concurrently to the bared oxygen atom, recovering the hydroxyl moiety and forming *ipso*-CT isomer. This *concerted* isomerization channel is 20 kcal mol^{-1} more favorable than alternatively proposed pathways.[28] Formation of the same *ipso*-CT product presented by the authors proceeds via the H-transfer of one OH-group to the neighboring carbon atom bearing another hydroxyl group (noted as TSQ5[28]). This H-transfer pathway was calculated in our previous work[25,26] to have a much higher barrier of activation (87 kcal mol^{-1} vs 66 kcal mol^{-1} at 0 K). (cf. Scheme 1 and TS4′ vs TS4). In fact, the lowest energy channel, the transformation of CT to *ipso*-CT isomer, is missing in RRKM calculations, where it was suggested the lowest energy reaction channel is formation of α-CT.[27,28]

Remarkably, *ipso*-CT also has an option of ring-fission with a barrier of 30 kcal mol^{-1} (Rxn 5), which is much more feasible than the simple bond cleavage (via TS5, Scheme 1).

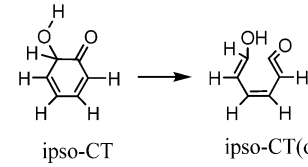

(5)

However, as shown in Scheme 1, the reverse barrier is only 5.9 kcal mol^{-1}, and the equilibrium is shifted back to the formation of *ipso*-CT. Therefore, other pathways involving this *ipso*-CT isomer are dominant (vide infra).

H_2O Elimination. We have localized three main channels for H_2O elimination from CT (Rxns 6−8, Scheme 2). Reaction

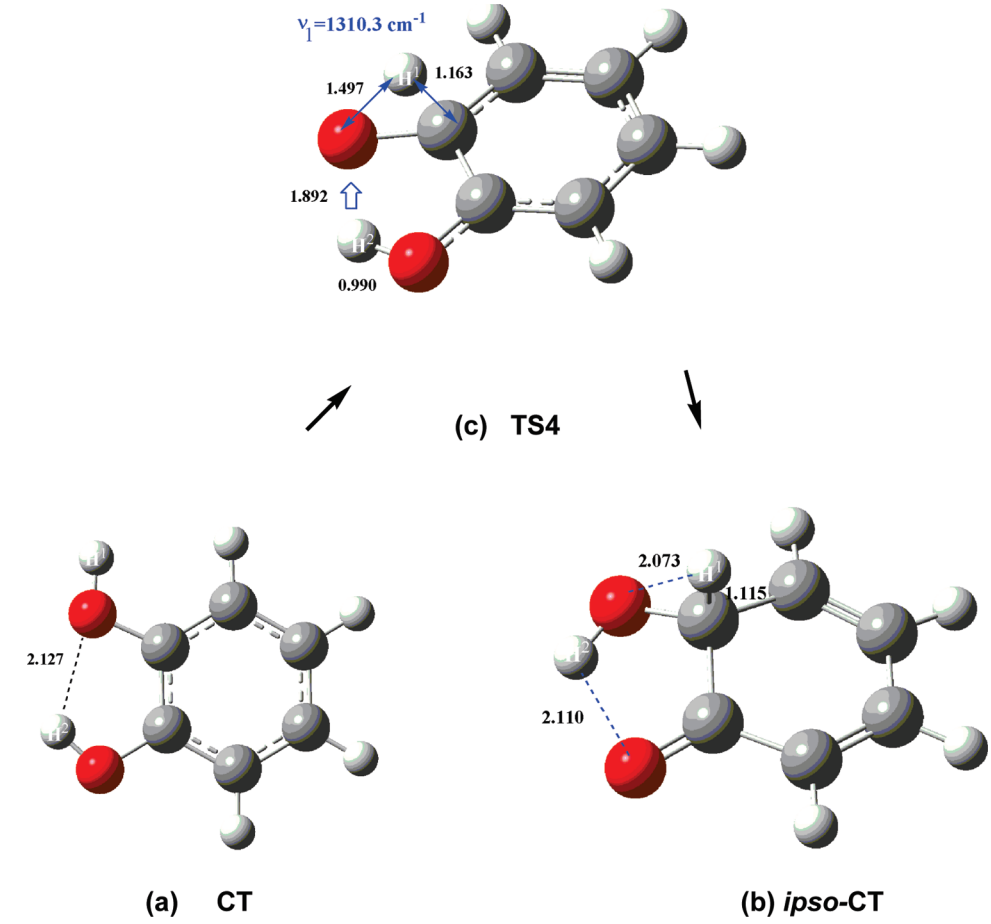

Figure 3. The concerted isomerization of catechol (a), to *ipso*-CT (b), through transition state structure (c) calculated at the CBS-QB3 level. Intrinsic reaction coordinate analysis shows that while the H^1 atom of the OH^1-group of CT transfers to *ipso* carbon, the H^2 atom of the neighboring OH^2-group migrates to the now available oxygen atom, recovering the hydroxyl moiety and forming the *ipso*-CT isomer.

SCHEME 2

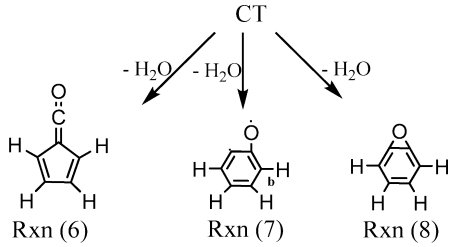

SCHEME 3

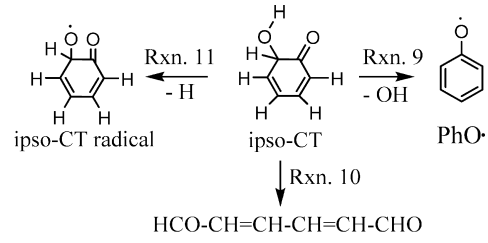

6, corresponding to the formation of a five-membered cyclic compound via TS6 in Scheme 1, is moderately endothermic with $\Delta H_{rxn6} = 34.4$ kcal mol^{-1}, and a CBS-QB3 calculated activation energy of 81.8 kcal mol^{-1} at 298 K (80.7 kcal mol^{-1} at the single level calculation). The substantially lower 77.2 kcal/mol activation energy for Rxn 6 based on B3LYP is used in RRKM calculations, which would result in a greater contribution of this reaction at higher temperatures.[28]

The spin-forbidden Rxn 7 leading to the formation of a triplet biradical is less endothermic with the $\Delta H_{rxn7} = 76.7$ kcal mol^{-1} at the B3LYP level. However, at higher levels of calculation this value is increased to 82.3 kcal mol^{-1}.

Concerted elimination of water via Rxn 8 results in the formation of benzene epoxide, which is probably in equilibrium with its diradical.[12] However, Rxn 8 exhibits very high activation energy of 98.3 kcal mol^{-1} according to the CBS-QB3 calculations and would be feasible only at higher temperatures.

Secondary Reactions. The pathways highlighted in green in Scheme 1 refer to the secondary conversions of CT isomers: their dissociation to radicals, isomerization processes, and other key reactions.

The dissociation channel for *ipso*-CT isomer to PhO• and •OH (Rxn 9, Scheme 3) is a potentially important reaction with substantial entropy gain. Evaluated at the CBS-QB3 level, the BDE is 64 kcal mol^{-1}, which is 6.0 kcal mol^{-1} higher than the value predicted at B3LYP level (58.0 kcal mol^{-1}, Scheme 1). Reaction 10 transforms *ipso*-CT to the open dialdehyde (HCO−CH=CH−CH=CH−CHO) via TS10 with activation barrier of 94.1 kcal mol^{-1}. Under pyrolytic conditions, the *ipso*-CT and α-CT may also undergo further unimolecular dissociation via O−H bond scission. (Rxn 11, Scheme 3, and Rxn 12).

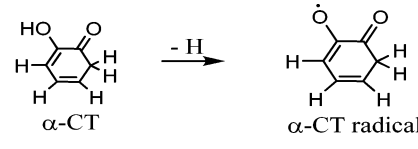

(12)

SCHEME 4

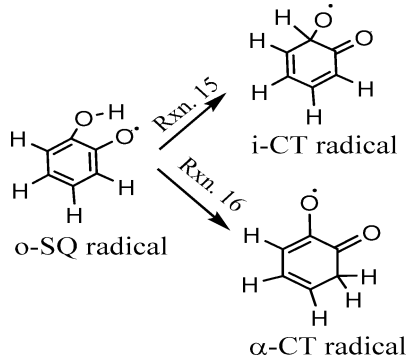

Direct O−H dissociation in *ipso*-CT is much higher in energy ($\Delta H_{rxn,11}$ = 103.1 kcal mol^{-1}) than in α-CT to α-CT radical (ΔH_{rxn12} = 82.2 kcal mol^{-1}). Instead, the loss of a hydrogen atom from the sp^3 ring carbon atom appears to be the energetically favored reaction ($\Delta H_{rxn13(298)}$ = 50.0 kcal mol^{-1} and $\Delta H_{rxn14(298)}$ = 62.3 kcal mol^{-1}).[25,26] Thus, among the secondary reactions, the conversion of *ipso*-CT to the oxygen-centered isomer of *o*-SQ radical is the most feasible pathway (Rxn 13).

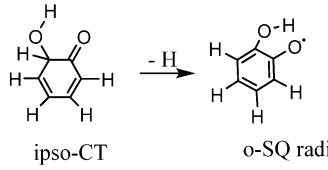

(13)

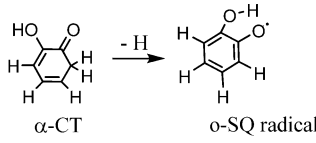

(14)

The *o*-SQ radical can further isomerize to *ipso*-CT radical and α-CT radical via Rxns 15 and 16 in Scheme 4 (cf. TS15 and TS16 in Scheme 1), respectively. Isomerization of *o*-SQ radical to *ipso*-CT radical (Rxn 15, Scheme 4) exhibits a high activation barrier of 70 kcal mol^{-1} via TS15 (the reverse barrier is 16.8 kcal mol^{-1}) compared to the direct O−H bond cleavage to *o*-BQ of 73.2 kcal mol^{-1} at the same B3LYP level of theory (vide supra). Transformation of *o*-SQ radical to α-CT radical (Rxn 16, Scheme 4) has a similar barrier of 71.7 kcal mol^{-1} (Scheme 1).

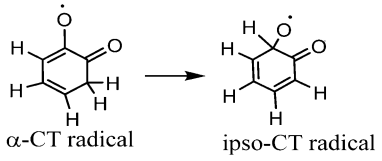

(*via* TS17) (17)

Isomerization of α-CT radical into *ipso*-CT radicals proceed with a low barrier of 42.3 kcal mol^{-1}.

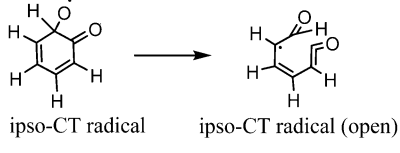

(*via* TS18) (18)

Ipso-CT radical can be readily transformed back to α-CT radical with a barrier of 10.2 kcal mol^{-1} or undergo very low barrier ring fission (2.5 kcal mol^{-1}, TS18, Scheme 1) to the open *ipso*-CT radical via Rxn 18.

Despite the relatively low barrier of 50 kcal mol^{-1} for Rxn 13, one would expect that *ipso*-CT does not form *o*-SQ radical via a unimolecular pathway, as it has an alternative option to break a weak ring C−C bond through a substantially lower barrier of 30 kcal mol^{-1} (Rxn 5). However, the reverse reaction barrier, as seen in Scheme 1, is even (5.9 kcal mol^{-1}), and apparently the equilibrium between open and cyclic structures of *ipso*-CT will be shifted toward the *ipso*-CT isomer. This provides an opportunity to transform *ipso*-CT to the *o*-SQ radical by Rxn 13 as well as to decompose partially into phenoxyl and hydroxyl radicals (Rxn 9), which is also favored entropically.

The role of open *ipso*-CT molecule can be significant at high temperatures by direct dissociation of *ipso*-CT (open) to *ipso*-CT radical (open) via Rxn 19 ($\Delta H_{rxn,19}$ = 67.0 kcal/mol). The *ipso*-CT (open) radical can also be formed via bimolecular reaction with pool radicals.

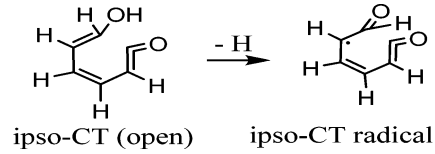

(19)

The fate of the open radical is not addressed here in detail, but one of the feasible decomposition channels is elimination of HCO and the formation of cyclopentadienone via Rxn 20 ($\Delta H_{rxn,20}$ = 32 kcal mol^{-1}).

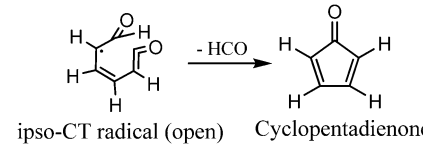

(20)

Another reaction pathway for *ipso*-CT radical (open) is decomposition to acetylene and CO or vinyl acetylene and CO. As one of the major products of pyrolysis of CT,[11] this suggests *ipso*-CT isomer will have significant input into the product distribution.

It is also important to note the possible conversion of *o*-BQ to the open molecule by Rxn 21 (ring fission via TS21) with a low activation barrier of 38.1 kcal mol^{-1} calculated at the B3LYP/6-31G(d,p) level.

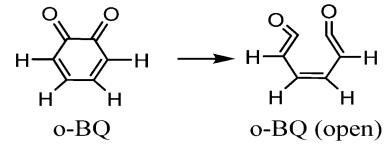

(21)

For most bond dissociation reactions considered here, B3LYP underestimates dissociation energies by 4−8 kcal mol^{-1}, whereas the barrier heights calculated using the same basis sets are underestimated to a lesser degree (2−4 kcal mol^{-1}), likely due to basis set superposition errors in single level calculations.

4. Conclusions

In conclusion, based on a series of experimental works performed in our laboratory we can state that CPD radicals are the dominant radical above 800 °C for both CT and HQ.[22,23,25,35] The semiquinone radicals, *p*-SQ and *o*-SQ formed from the gas-phase pyrolysis of HQ and CT, respectively, are the dominant radical products below 750 °C. However, *p*-BQ was the main product from HQ pyrolysis[13] whereas *o*-BQ product was not observed from pyrolysis of CT.[12] These results, in combination with the high concentrations of *o*-SQ radicals detected from pyrolysis of CT[25] suggest new isomerization pathways (Scheme 1) are operable in CT that are not present in HQ.[22,35]

The absence of o-BQ as a catechol pyrolysis product might also be explainable by existence of additional decomposition pathways of *o*-SQ radical (for instance CO elimination from *o*-SQ radical)[25,27,28] However, high calculated activation energies for elimination of CO from semiquinone radicals have been reported in the literature, namely, 58−65.1 kcal mol^{-1} for *p*-SQ radical and 63.1−74.4 kcal mol^{-1} for *o*-SQ radical.[36,27] These values are much higher than the reported values for expulsion of CO from phenoxyl radical of 44−48 kcal/mol (experimental)[37] and 52−61.6 kcal/mol (calculated).[36,38] These differences suggest the decomposition of semiquinones is not as important as phenoxyl. Thus, it is also important to include all the reactions considered in this and other recent publications[25,27,28] to explain the product distributions from CT, especially the formation of *ipso*-CT (this work).

Acknowledgment. The authors gratefully acknowledge the partial support of this research under NSF Grant CTS-0317094.

References and Notes

(1) Dellinger, B.; Pryor, W. A.; Cueto, R.; Squadrito, G. L.; Deutsch, W. A. *Organohalogen Compd.* **2000**, *46*, 302.
(2) Dellinger, B.; Pryor, W. A.; Ceuto, R.; Squadrito, G. L.; Hedge, V.; Deutsch, W. A. *Chem. Res. Toxicol.* **2001**, *14*, 1371.
(3) Pryor, W. A.; Terauchi, K.; Davis, W. H. *Environ. Health Perspect.* **1976**, *16*, 161.
(4) Pryor, W. A.; Prier, D. G.; Church, D. F. *Environ. Health Perspect.* **1983**, *47*, 345.
(5) Schlotzhauer, W. S.; Martin, R. M.; Snook, M. E.; Williamson, R. E. *J. Agric. Food Chem.* **1982**, *30*, 372.
(6) Pryor, W. A.; Stone, K.; Zang, L.-Y.; Bermudez, E. *Chem. Res. Toxicol.* **1998**, *11*, 441.
(7) Halliwell, B. B.; *Cigarette Smoke and Oxidative Stress*; Poulsen, H. E.; Eds.; Springer-Verlag: Berlin Heidelberg, 2006.
(8) Lynch, B. M.; Durie, R. A. *Aust. J. Chem.* **1960**, *13*, 567.
(9) Elliot, D. C. *J. Am. Chem. Soc.* **1988**, 55.
(10) Sakai, T.; Hattori, M. *Chem. Lett.* **1976**, 1153.
(11) Ledesma, E. B.; Marsh, N. D.; Sandrowitz, A. K.; Wornat, M. J. *Proc. Combust. Inst.* **2002**, *29*, 2299.
(12) Truong, H.; Lomnicki, S.; Dellinger, B. *Chemosphere* **2008**, *73*, 629.
(13) Truong, H.; Lomnicki, S.; Dellinger, B. *Chemosphere* **2008**, *71*, 107.
(14) Shin, E.-J.; Hajaligol, M. R.; Rasouli, F. *Fuel* **2004**, *83*, 1445.
(15) Pryor, W. A.; Prier, D. G.; Church, D. F. *Environ. Health Perspect.* **1983**, *47*, 345.
(16) Pryor, W. A. *Environ. Health Perspect.* **1997**, *105*, 875.
(17) Wornat, M. J.; Ledesma, E. B.; Marsh, N. D. *Fuel* **2001**, *80*, 1711.
(18) Ledesma, E. B.; Marsh, N. D.; Sandrowitz, A. K.; Wornat, M. J. *Energy Fuels* **2002**, *16* (6), 1331.
(19) Marsh, N. D.; Ledesma, E. B.; Sandrowitz, A. K.; Wornat, M. J. *Energy Fuels* **2004**, *18* (1), 209.
(20) Truong, H. Ph.D. Dissertation, Copper (II) oxide mediated formation and stabilization of combustion generated persistent free radicals, Louisiana State University: Baton Rouge, 2007.
(21) Thomas, S.; Wornat, M. J. *Fuel* **2008**, *87*, 768.
(22) Adounkpe, J.; Khachatryan, L.; Dellinger, B. *Energy Fuels* **2008**, *22*, 2986.
(23) Khachatryan, L.; Adounkpe, J.; Dellinger, B. *Energy Fuel* **2008**, *22*, 3810.
(24) Khachatryan, L.; Adounkpe, J.; Maskos, M.; Dellinger, B. *Environ. Sci. Technol.* **2006**, *40*, 5071.
(25) Khachatryan, L.; Adounkpe, J.; Asatryan, R.; Dellinger, B. *J.Phys. Chem., A* **2010**, *114*, 2306.
(26) Khachatryan, L.; Adounkpe, J.; Asatryan, R.; and Dellinger, B. 11th International Congress on Combustion by-Products and Their Health Effects, Research Triangle Park, May 31st to June 3rd, 2009.
(27) Altarawneh, M.; Dlugogorski, B. Z.; Kennedy, E. M.; Mackie, J. C. *J.Phys. Chem., A* **2010**, *114*, 1098.
(28) Altarawneh, M.; Dlugogorski, B. Z.; Kennedy, E. M.; Mackie, J. C. *J.Phys. Chem., A* **2010**, *114*, 1060.
(29) Becke, A. D. *J. Chem. Phys.* **1993**, *98*, 5648.
(30) Lee, C.; Yang, W.; Parr, R. G. *Phys. Rev. B* **1988**, *37*, 785.
(31) Frisch, M. J. Trucks, G. W.; Schlegel, H. B.; Scuseria, G. E.; Robb, M. A.; Cheeseman, J. R.; Montgomery, Jr., J. A.; Vreven, T. K.; , K. N.; Burant, J. C.; Millam, J. M.; Iyengar, S. S.; Tomasi, J.; Barone, V.; Mennucci, B.; Cossi, M.; Scalmani, G.; Rega, N.; Petersson, G. A.; Nakatsuji, H.; Hada, M.; Ehara, M.; Toyota, K.; Fukuda, R.; Hasegawa, J.; Ishida, M.; Nakajima, T.; Honda, Y.; Kitao, O.; Nakai, H.; Klene, M.; Li, X.; Knox, J. E.; Hratchian, H. P.; Cross, J. B.; Adamo, C.; Jaramillo, J.; Gomperts, R.; Stratmann, R. E.; Yazyev, O.; Austin, A. J.; Cammi, R.; Pomelli, C.; Ochterski, J. W.; Ayala, P. Y.; Morokuma, K.; Voth, G. A.; Salvador, P.; Dannenberg, J. J.; Zakrzewski, V. G.; Dapprich, S.; Daniels, A. D.; Strain, M. C.; Farkas, O.; Malick, D. K.; Rabuck, A. D.; Raghavachari, K.; Foresman, J. B.; Ortiz, J. V.; Cui, Q.; Baboul, A. G.; Clifford, S.; Cioslowski, J.; Stefanov, B. B.; Liu, G.; Liashenko, A.; Piskorz, P.; Komaromi, I.; Martin, R. L.; Fox, D. J.; Keith, T.; Al-Laham, M. A.; Peng, C. Y.; Nanayakkara, A.; Challacombe, M.; Gill, P. M. W.; Johnson, B.; Chen, W.; Wong, M. W.; Gonzalez, C.; and Pople, J. A. *Gaussian 03, Revision D.01*; Gaussian, Inc.: Wallingford CT, 2004.
(32) Montgomery, J. A., Jr.; Frisch, M. J.; Ochterski, J. W.; Petersson, G. A. *J. Chem. Phys.* **1999**, *110*, 2822.
(33) (a) Asatryan, R.; Bozzelli, J. W. *J. Phys. Chem. A* **2010**, *114*, 7693–7708. (b) Asatryan, R.; Bozzelli, J. W.; Da Silva, G.; Nguyen, M. T.; Swinnen, S. *J. Phys. Chem. A* **114**, 6235–6249. (c) Asatryan, R.; Da Silva, G. J. W. B. *J. Phys. Chem. A.* **2010**, *114*, 8302−8311. (d) Hudzik, J. M.; Asatryan, R.; Bozzelli, J. W. *J. Phys. Chem. A.* **2010**, in press. (e) Asatryan, R.; Bozzelli, J. W. *Phys. Chem. Chem. Phys.* **2008**, *10*, 1769−1780.
(34) (a) Borges dos Santos, R. U.; Martinho Simoes, J. A. *J. Phys. Chem. Ref. Data* **1998**, 707–741. (b) Fattahi, A.; Kass, S. R.; Liebman, J. F.; Matos, M. A. R.; Miranda, M. S.; Morais, V. M. S. *J. Am. Chem. Soc.* , *127*, 6116.
(35) Dellinger, B.; Lomnicki, S.; Khachatryan, L.; Maskos, Z.; Hall, R.; Adounkpe, J.; McFerrin, C.; Truong, H. *Proc. Combust. Inst.* **2007**, *31*, 521.
(36) McFerrin, C. A.; Hall, R. W.; Dellinger, B. *THEOCHEM* **2008**, *848*, 16.
(37) Lin, C.-Y.; Lin, M. C. *Int. J. Chem. Kin.* **1985**, *17*, 1025.
(38) Liu, R.; Morokuma, K.; Mebel, A. M.; Lin, M. C. *J. Phys. Chem.* **1996**, *100*, 9314.

JP1054588